UCRL-99353
PREPRINT

HIGH-FREQUENCY SEISMIC OBSERVATIONS AND MODELS OF CHEMICAL EXPLOSIONS: IMPLICATIONS FOR THE DISCRIMINATION OF RIPPLE-FIRED MINING BLASTS

Albert T. Smith

This paper was prepared for submittal to the Bulletin of the Seismological Society of America.

August 8, 1988

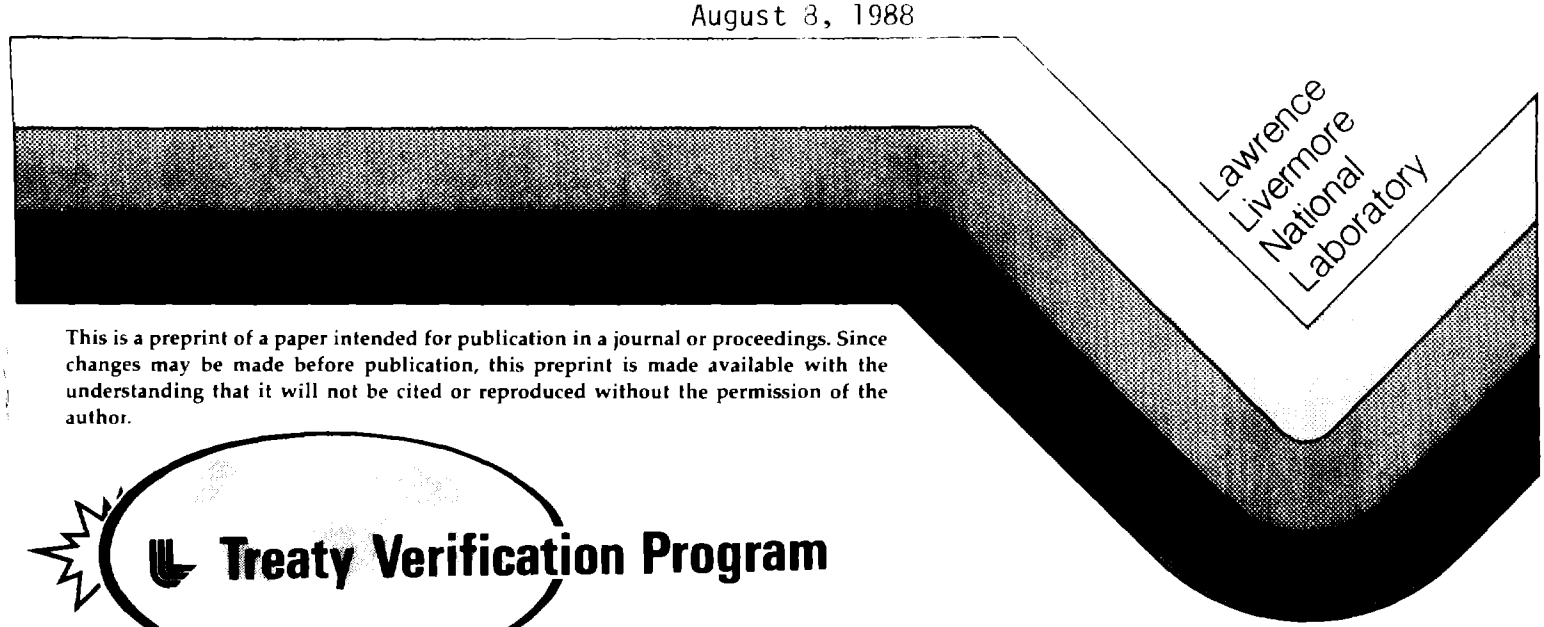

High-Frequency Seismic Observations and Models of Chemical Explosions: Implications for the Discrimination of Ripple-Fired Mining Blasts

Albert T. Smith
Lawrence Livermore National Laboratory
P.O. Box 808, Livermore, CA 94550

August 8, 1988

Submitted to the *Bulletin of the Seismological Society of America*

ABSTRACT

Discrimination of large chemical explosions (*e.g.*, mining blasts) from possible clandestine nuclear tests (*e.g.*, decoupled-explosions) is a significant issue for seismic verification. Unless discrimination is possible, the numerous mining blasts within the USSR would give ample opportunity for concealing a clandestine test. Evernden *et al* (1986) advocate high frequencies as a means to detect these clandestine tests; however, mining blasts must still give a unique signature for their discrimination. Specific conditions are also necessary for high-frequency verificatior: low attenuation and *quiet* seismic stations are among the most important. In this study we address these problems under conditions representing a best case scenerio.

During the summer of 1985, LLNL deployed a regional array and high frequency seismic station near RSON (Red Lake, Ontario, Canada) to study regional seismic signals at a *low-noise* site with excellent propagation characteristics, the continental shield. One objective was to evaluate the performance of regional seismic arrays and high-frequency stations in this geological environment. Using high-frequency data from mining blasts within the Masabi Iron Range in northern Minnesota (distance of 380 km), we also observed the high-frequency P_n phase of ripple-fired blasts, modelled their source properties, and evaluated a possible discriminant for chemical explosions.

This study suggests the existence of a distinctive signature for large chemical explosions: strong, high-frequency spectral peaks in the P spectra introduced by delay shooting or ripple-firing. Its application depends, however, on a frequency band extending to at least 35 Hz at regional distances, reasonably uniform delay times in the blast pattern, predictably *quiet* seismic sites, and minimal path attenuation for high frequencies. At 380 km, we observe good propagation to 30 Hz; at 50 Hz the evidence suggests severe attenuation or scattering which is consistent with a total Q between 1500 and 2500. Attenuation estimates assuming a simple source behavior (*e.g.* f^{-2} or f^{-3}) at high frequencies for mining explosions would give incorrect values of Q unless corrected for the blast pattern. These attenuations will limit the value of high-frequencies for the detection of small decoupled explosions at regional distances.

Introduction

A major issue for a Low-Yield Threshold Test Ban Treaty or a Comprehensive Test Ban Treaty is the discrimination of large chemical explosions from possible clandestine nuclear tests (*e.g.*, nuclear explosions decoupled in large underground cavities). High frequency seismology has been advocated as a means to detect these clandestine tests (Evernden *et al*, 1986); however, a large number of chemical explosions must still be discriminated from small nuclear detonations. The importance of chemical explosions for discrimination was recognized in the Vela Uniform Program with both observations and interpretation of quarry blasts (Willis, 1963; Pollard, 1963; Frantti, 1963). These rippled-fired chemical explosions may produce a unique spectral signature and the recognition of these features may facilitate discrimination of chemical from nuclear explosions. But two conditions are necessary for high-frequency verification: predictable noise and low attenuation for regional signals. In this study we address these problems under ideal conditions: a *quiet* site with propagation in a continental shield. Using high-frequency data from mining explosions, we can then observe the high-frequency signature of ripple-fired mining blasts, determine the mechanism generating the signature, and evaluate its potential as a discriminant for chemical explosions.

The Red Lake, Ontario station (*RSON*) of the Regional Seismic Test Network (*RSTN*) is considered representative of a shield environment and a *low-noise* site (Taylor, 1981; Rodgers *et al*, 1987; Smith, 1987; Smith and Grose, 1987). Seismograms recorded at RSON during 1984 indicate numerous mining explosions from the Mesabi Iron Range in northern Minnesota at 380 km. These are ideal sources for high-frequency studies of chemical explosions and path propagation across continental shields. During the summer of 1985 a small regional array and a high frequency station were emplaced 5 km from the RSON station to pursue these investigations and to evaluate the performance of regional seismic arrays in this geologic environment (Smith, 1986).

High-Frequency Site and Instrumentation

The selection procedure for the high-frequency site incorporated observations of signals and noise from the regional array. Data from each element of the array were reviewed for low background noise, signals free from site reverberations (ringing), and optimum signal-to-noise ratio (*SNR*). The array itself was constrained to an area of relatively flat topography near RSON. The evaluation of high-frequency sites was primarily confined to

outcrops of granitic shield, but data was also reviewed from sites with thin sedimentary or alluvial cover. A fresh but unused quarry proved to be the optimum high-frequency site within the area of good SNR. Figure 1 shows the location of the high-frequency site, the location of the regional array, and the RSON station.

The high-frequency station used a Teledyne Geotech S-750 accelerometer and an event-triggered Kinemetrics PDR-2 digital recorder. The S-750 seismometer was designed for extremely low background noise and was the short-period seismometer within RSTN. The seismometer was grouted to bedrock within a two foot hole. In this position at the bottom of the quarry, the seismometer was approximately 30 feet below the surrounding surface. The instrument was at least 100 feet from any vegetation and was decoupled from their wind induced vibrations by the intervening glacial till. Together with the sheltered location of the seismometer, this strategy minimized wind noise.

The PDR-2 digital recorder sampled at 500 Hz, used a 2 pole anti-aliasing filter at 125 Hz, and was triggered from a second PDR-2 attached to a small array. This triggering array consisted of three S-13 velocity sensors separated by 350 meters in a tripartite pattern. Each was connected by cable to a central PDR-2 which required all sensors to simultaneously observe an event before the recorder would issue a trigger. The evaluation was based on the ratio of the short-term average to the long-term average. The digital recorder attached to the array was the master and simultaneously triggered the slave recorder, the PDR-2 with the S-750 seismometer, when an event was detected. Since velocity sensors were utilized in the triggering array, the system was most sensitive to events with significant energy between 1 and 10 Hz, which may not be optimum for some regional events. The array eliminated most triggers from moving noise sources such as automobiles and from noise sources localized to one seismometer site. But to guarantee acquisition of the high-frequency P_n phase from ripple-fired explosions, data from the seismometers was recorded continuously when blasts were scheduled at specific mines.

Sufficient gain was applied to give maximum resolution to background noise without gain ranging the PDR-2 recorder. Using acceleration effectively pre-whitened the noise and signal; thus, high-frequencies were not lost in bit or quantization noise. There was also no evidence of aliasing in the data when sampled at 500 Hz with the anti-aliasing filter at 125 Hz. No attempt was made to remove the effect of the anti-aliasing filter since our analysis involves frequencies lower than 100 Hz.

Principles of Ripple-Fired Explosions

Ripple-fired explosions are the accepted practice for fragmenting rock during quarry and open-pit mining. Ripple-firing (*or delay-shooting*) optimizes the fragmentation of rock and minimizes the seismic disturbance of nearby structures (Langefors and Kihlstrom,

1963); therefore, most large chemical explosions use this approach. The periodicity inherent in ripple-firing produces a seismic reinforcement at the frequency of the delay between rows. Observations during the Vela Uniform Program did not resolve high-frequency reinforcements but considered them as outside the usable seismic passband at regional distances (Willis, 1963; Pollard, 1963; Frantti, 1963). Near-field data and modelling did treat the principles of ripple-firing and its spectral reinforcements. This analysis is further explored by Greenhalgh (1980), but again with emphasis on seismic frequencies lower than 10 Hz. In this section I explore high-frequency source characteristics of ripple-firing and compare these results to our regional data. Unlike other approaches, the analysis incorporates the effect of the blast's spatial distribution on spectral reinforcements.

Ripple-firing or delay-shooting can be viewed as a sequence of single explosions arranged and fired in a pattern using a series of time-delayed detonations between adjacent shot holes or rows of shot holes. When shooting the face of a bench, the delay time allows the previous row to fragment the rock and blast it away from the face before the next row detonates. As a source, we could view this as the convolution of a single explosion with a comb function of variable spacing and variable amplitude (which depends upon the number of simultaneous shots and their explosive charge). If the source for a single explosion is reproducable from hole to hole, we can assume one source function for all explosions. Anderson *et al* (1982) confirm the latter assumption during their observations of quarry blasts.

First we examine the effect of ripple-firing on a sequence of shots at a single location. This is equivalent to ignoring the finite spatial extent of an actual quarry blast, a reasonable assumption if the product of the seismic velocity with the time delay between shots is much larger than the blast pattern. Using $u(t)$ as the seismic signal from a single shot and $U(f)$ as its Fourier transform (*or spectrum*), and assuming a constant time delay δ_t between each shot or set of simultaneous shots (*e.g.* a row of shots), then the signal $s(t)$ from the ripple-fired blast is the sum of all N shots or rows:

$$s(t) = \sum_{m=0}^{N-1} r(m\delta_t)u(t - m\delta_t) \tag{1}$$

where $r(m\delta_t)$ represents the number of charges at time $m\delta_t$ from the initiation of the blast. If time delays between shots are not uniform, we can represent this as a continuous integral:

$$s(t) = \int_{\tau=0}^{t_N} r(\tau)u(t - \tau) \tag{2}$$

where t_N is the total duration of the blast and $r(\tau)$ describes either the number of charges exploding at a specific time τ or the total size of the charges initiated at time τ. Normally,

this would be an uneven comb function, each spike representing one shot hole or multiple holes fired at time τ. The amplitude of the spike reflects the total size of the shots fired at that instant. These equations represent the discrete convolution of two functions, the source function $u(t)$ for a single shot and the delay-time function $r(t)$ for the shooting pattern:

$$s(t) = r(t) * u(t) \tag{3}$$

By the convolution theorem, our source spectrum $S(f)$ for the ripple-fired blast becomes the product of a single shot spectrum $U(f)$ and the spectrum $R(f)$ of the firing sequence:

$$S(f) = R(f) \cdot U(f) \tag{4}$$

Ripple-firing modulates the spectrum of a single shot, reinforcing some frequencies and suppressing others; thus, the temporal firing pattern determines the unique signature of ripple-fired explosions.

To illustrate these underlying principles, let us consider two models, one an infinite sequence of δ-functions representing an evenly spaced (interval δ_t) sequence of explosions, and the other a box-car function of unit height and length t_N. An infinite comb function, $\prod(\delta_t)$, is our first model. This is analogous to an infinite sequence of shots, each separated in time by δ_t. Its fourier transform is another comb function in the frequency domain, $\prod(\frac{1}{\delta_t})$, where the δ-spikes occur at frequencies of 0, $\frac{1}{\delta_t}$, $\frac{2}{\delta_t}$, ... (*e.g.* Brigham, 1974). Thus, spectral peaks or reinforcements occur at the fundamental and harmonics of $\frac{1}{t_\delta}$. But the mining blasts are not an infinite sequence; they are of finite duration. The finite duration is analogous to the application of a box-car function; it introduces a finite width, $\frac{2}{t_N}$, to the spectral peak and low-amplitude ripples between the periodic peaks as shown in Figure 2. The essential feature of strong spectral reinforcements remains, but incomplete cancelation occurs between peaks. In practice, the temporal firing sequence, the spatial pattern, and the resulting spectrum are more complex.

The spatial pattern of the shot holes introduces additional time delays. These delays accumulate within rows as well as between rows. Assuming a uniform half space of velocity v, uniform shot elevation, and coordinates x_i and y_i for shot hole i, the additional delay is proportional to the projection of the vector $(x, y, 0)$ onto the unit vector lying along the ray or propagation direction. For a station lying at azimuth z and take-off angle θ from vertical, the total time delay t_i^δ for the ith shot hole becomes

$$t_i^\delta = \frac{\sin\theta}{v}\sqrt{x_i^2 \sin^2 z - y_i^2 \cos^2 z} + t_i \tag{5}$$

where t_i is the shot's time delay relative to the initiation point. Since these delays and coordinates are specified relative to the blast's initiation point, the total time delay t_i^δ can

be negative. The charge for each shot is cummulatively summed at the specified delay into the delay function $r(t)$.

These principles allow us to predict the spectral modulations introduced by ripple-firing known blast patterns. The next section reviews data from three known chemical explosions in the Mesabi Range and explores their relationship to the predicted behavior using both the basic principles and the complete spatial blast pattern.

Regional Signals and Modelling of Mining Explosions

Signal characteristics and background noise determine our ability to detect an event, whether explosion or earthquake. The source determines the intrinsic excitation of specific seismic phases, their spectral content, and their radiation pattern; the signal is then distorted (or filtered) as it propagates through the earth. The local site conditions play a key role since much of the signal distortion and attenuation occurs within the near surface layers (*e.g.*, Bouchon, 1982; Frankel and Wennerberg, 1987). These factors combine to determine the final signal characteristics at our seismometer and, with the characteristics of the seismic noise, determine the necessary specifications for optimum performance of our seismic system. In this section we review the spectral characteristics of explosion signals recorded at our high-frequency station, model the source properties of these ripple-fired blasts, and consider their significance for the detection, location, and discrimination of chemical explosions.

Discrimination depends upon a unique signature for underground nuclear explosions, chemical explosions, and earthquakes. Mine explosions from the Mesabi Iron Range in Minnesota give sources for both propagation studies and source studies of chemical explosions. These are large, ripple-fired blasts in open pit mines for which specifics on blast pattern and delays are available. Mining explosions within the Mesabi Range are commonly shot with 17 to 65 ms delays between the individual rows. If spectral reinforcements originate in this periodicity, they should be readily observed from mines with known delay and shooting patterns. Table 1 gives data on three mine explosions, including their primary delay time between rows, approximate locations, and origin time. These explosions are designated as A, B, and C. Figure 3 illustrates a series of bandpasses for two explosions, A and C. The first, explosion A, illustrates the significance of spectral reinforcements on P_n: delay-shooting can increase dramatically the signal-to-noise ratio (SNR) at high frequencies. At lower frequencies, L_g and R_g are both prominent arrivals. But P_n is only strong in the bandpass from 16 to 32 Hz, which corresponds to the predominant frequency of ripple-firing in Table 1.

Not all explosions show this unusual behavior, as Figure 3b demonstrates. Explosion C

triggered our event recorder and produced the largest amplitudes of any explosion recorded from the Mesabi Range. Large P_n and P_g phases triggered the initial 50 second; subsequently, the S_n and L_g phases triggered an additional 50 seconds, which included R_g. This explosion was unusual in its short duration, 200 ms; short delays between rows, 17 ms; and total explosive power, 130,000 kg. In terms of explosive detonated per millisecond, this blast was by far the largest recorded by our field deployment. P_n now has its best SNR at much lower frequencies, 4 to 8 Hz, and shows a prominent P_g phase. These characteristics may be associated with the short delay time, equivalent to a 59 Hz reinforcement. The spectral characteristics of these P_n phases and the firing pattern for the responsible explosion provide essential information on propagation characteristics, assist interpretation of possible discriminants, and allow detailed modelling of ripple-firing.

P_n spectra for explosions in Table 1 illustrate the consequences of ripple-firing with different delay times between the rows. Figure 4 shows spectra for all three explosions. The first two explosions, A and B, show strong spectral peaks indicative of ripple-firing. Explosion A shows a strong spectral peak at 26 Hz, which coincides with the maximum SNR as seen in Figure 3a. Apparently, we are observing spectral reinforcements from rows of explosives fired sequentially with delays of 35 ms. Explosion B also has a spectral reinforcement but is located at 20 Hz, which agrees with the dominant 50 ms delay between rows. These spectral reinforcements are not artifacts of the site response; the explosions are all approximately 380 kilometers from our seismic station and are at similar azimuths. Instead, these spectra reflect primary source characteristics, the delay time and its regularity in the blast pattern.

Not all mine blasts have distinctive spectral peaks, as explosion C demonstrates in Figure 4c. A delay time of 17 ms between rows should produce a spectral reinforcement at 59 Hz, but none is apparent. Instead, we observe a rapid decrease of high frequencies (f^{-4} in displacement amplitude) above an apparent corner frequency near 8 Hz. The total duration of 200 ms for the ripple-fired shot implies that, for frequencies less than 5 Hz, the explosion should have the appearance of a single, instantaneous explosion; the 200 ms duration of the explosion should introduce a corner frequency near 5 Hz. According to the Sharpe model, the displacement amplitude for a single explosion should decrease at f^{-2} in displacement amplitude (Sharpe, 1942; von Seggern and Blandford, 1972). Instead, we observe f^{-4} for this ripple-fired mining blast. Any model must also explain the absence of the 59 Hz spectral reinforcement. Unlike the P_n signals for explosions A and B, a high-frequency station would not provide better detection capability than a RSTN station; for explosion C the best SNR occurs near the corner frequency at 8 Hz.

Differences between these three ripple-fired mining blasts may be a reflection of shooting practices: duration, explosive per millisecond, and delay time between rows. If the delay is short, say 17 ms as in blast C, the reinforcement may be outside of the seis-

mic band at regional distances. If the row delay is longer and coincides with the seismic band as for blasts A and B, a strong spectral peak may be observed. This behavior is quantitatively modelled in the next section.

An interesting comparison to our previous ripple-fired mining blast would be a single, well-coupled explosion. During our deployment near Red Lake, no single shots were recorded; however, RSNY (New York, RSTN station) recorded large refraction shots from Canada and Maine which were part of a U.S. Geological Survey project. The refraction shot shown in Figure 5 was a two ton explosion at the bottom of a water filled quarry in Canada and was 300 km from RSNY. Notice the distinct overshoot at 6 Hz; this was a common feature of all the refraction shots, whether in a borehole or at the bottom of a water filled quarry. At high frequencies, the roll-off was closer to f^{-3} in displacement amplitude; thus, high frequencies decreased more rapidly for our ripple-fired explosion.

In Figure 5, mining explosion C is also compared to a magnitude 4.4 earthquake which occurred on November 2, 1983. At 900 km the earthquake shows a slower decay at high frequencies than the closer explosion. This contradicts assertions and expectations about the behavior at high frequencies of a single explosion compared to the behavior of an earthquake at high frequencies: an explosion decays as f^{-2}, and an earthquake decreases as f^{-3} (*e.g.*, Evernden *et al*, 1986). But in Figure 5, the earthquake has a corner frequency near 4 or 5 Hz and rolls off as $f^{-2.5}$ at higher frequencies; the explosion decays as f^{-4} in displacement amplitude. The slower roll-off of the earthquake compared to the explosion must be a source effect; the earthquake is farther from RSON and would suffer greater high-frequency attenuation than the explosion. Although this is only one example, discrimination between this explosion and an earthquake would fail if only the slope at high frequencies is used as the criterion.

Our observations suggest, then, the presence of a unique signature for some large chemical explosions which could be exploited for discrimination. If the predominant frequency for ripple-firing lies within the seismic bandwidth at regional distances, spectral reinforcements result and provide a unique signature for discrimination of large chemical explosions. To verify these observations, we can apply our theoretical approximations for ripple-firing contained in the previous section, *Principles of Ripple-Fired Explosions*, to these mining blasts. Each mine responsible for an explosion in Table 1 has provided specific information on the blast pattern, charges, and delay times. This allows comparison of the observed to synthetic spectrum for each P_n arrival. In the following, I will show the results for two different cases: explosion B with strong spectral reinforcements, and explosion C with no evidence of reinforcements but having a rapid high-frequency decay in spectral amplitude.

Modelling Explosion B: 50 ms Delays

The mine blast, B, of August 7, 1985, has a particularly simple pattern and illustrates

strong spectral reinforcements for P_n (see Figure 4b). Figure 6a is a map view showing individual hole locations, the row configuration, and the time delays between individual rows. Each hole is approximately 10 m deep and contains approximately 400 kg. of explosive. The maximum charge per delay is 2,900 kg., and the average explosive per millisecond is 43 kg. for a total duration of 1.25 seconds.

Using this pattern and our previous derivation for $r(t)$ in equation (5) gives the ripple-firing delay function in Figure 6b for our station azimuth of 341°. Instead of one single spike for each row, the finite shot pattern introduces multiple lines at specific delay times (*e.g.* 0.51 seconds). The amplitude corresponds to the total cummulative charge per millisecond at a given delay time. The finite spatial pattern smears out each peak, which suppresses the higher frequency harmonics of the shooting frequency. The delay function $r(t)$ is dominated by the 50 ms row delays (20 Hz) except during the last 0.3 seconds when delays increase to 65 ms (16 Hz). The spectrum of the delay function should reflect these characteristics, a strong 20 Hz peak, and a minor reinforcement near 16 Hz.

Figure 6c shows spectra of the ripple-fired delay function $r(t)$ for two azimuths, 251° and 341°. These correspond to the azimuths for two RSTN stations, RSSD and RSON respectively. The dominant features are immediately apparent: a fundamental peak at 20 Hz and evenly spaced harmonics every 20 Hz, that is, 40 Hz, 60 Hz, 80 Hz; a low-frequency peak where the finite-duration appears as an instantaneous shot; additional reinforcements near 16 Hz and 32 Hz from 65 ms delays; and low-amplitude ripples between the peaks. Using this shooting pattern, negligible azimuthal effect is evident in the radiation pattern. In actual practice, the firing parameters can greatly vary from their nominal value (Winzer *et al*, 1979). Delay times may vary from the specified, single shots or even whole rows may not fire, and the burn rate within a borehole may vary by 50%. Models which include these effects and the propagation rate of the Primacord^{TM} from hole to hole within a row give only small perturbations to the spectra for frequencies less than 60 Hz. The primary effect is the suppression of high-frequency harmonics.

Explosions from single shot holes, as in Figure 5, produce a corner frequency between 5 and 10 Hz, and a high frequency roll-off of f^{-2} or greater in displacement amplitude. At high-frequencies, a good starting assumption is that a single shot within the blast pattern is flat to acceleration. Since the spectrum of the complete mine blast $S(f)$ is the product of the delay spectrum $R(f)$ and a single shot $U(f)$, we can view the delay function spectrum in Figure 6c as equivalent to acceleration power for frequencies greater than 5 to 10 Hz.

Our model at 351° shows the essential details observed in the P_n spectrum. Figure 6d compares the spectra from the model and data in units of acceleration power. The amplitude of the model spectra is scaled by 10^4 to give an approximate match to the spectral peak and minor ripples.

An excellent match is observed at the spectral peak and on either side of the peak. Notice the asymmetry of the peak; the acceleration power is greater above 25 Hz than between 5 and 15 Hz. The effect of 65 ms (16 Hz) delays is apparent between 15 and 20 Hz in both model and data; a hump occurs in the data spectrum near 18 Hz, while the model shows a corresponding feature between 15 and 18 Hz. Poor spectral resolution or variability of the nominal shooting characteristics could easily account for the difference. At frequencies lower than 5 Hz, the two diverge. These frequencies are lower than the corner frequency of a single explosion and thus reflect decreasing excitation of P_n at low frequencies - - the spectrum of a single shot is flat to displacement rather than acceleration. This comparison validates the essential features observed in ripple-fired mining blasts and our approach to their modelling.

Modelling Explosion C: 17 ms Delays

Not all ripple-fired mining explosions show reinforcements. The P_n spectrum from blast C on August 6 in Figure 4c shows no obvious spectral reinforcements; instead, the high frequencies rapidly decrease as f^{-4} in displacement amplitude. Information from the mine on this ripple-fired blast indicates two differences in their shooting practices: short delay times and strong irregularities in the blasting pattern. All the parameters significantly vary across the blast pattern in Figure 7a: depths of holes range from 8.5 to 18 m; charges per hole vary between 590 and 1900 kg.; delays are a short 9 to 17 ms; and the total duration of 207 ms is a factor of 5 to 10 less than most other mines in the Mesabi Range. The resulting maximum explosives per delay of *12,500* **kg.** and the average detonation per millisecond of 640 kg. greatly exceed those for blast B and account for the large amplitudes observed at 380 km.

The delay spectrum $R(f)$, denoted as Model in Figure 7b, shows a strong reinforcement near 52 Hz, a lower frequency than models which exclude the finite shot pattern. The short, 200 ms duration means that the blast appears as a single source and produces a constant spectral amplitude for frequencies lower than 5 Hz. Between 5 and 35 Hz, the individual rows and shots destructively interfere and a relative minimum occurs in the spectrum.

Comparing the model at 341° to the P_n spectrum for blast C requires a more speculative interpretation. Both the P_n spectrum and the delay spectrum $R(f)$ in Figure 7b use a 2 second window; the delay spectrum has again been scaled by 10^4 as in the previous blast on August 7. The spectrum for a single shot $U(f)$ has a corner frequency at 6 Hz, a high-frequency asymptote which is flat to acceleration, and a low-frequency asymptote flat to displacement. Our model source spectrum, $S(f)$, is the product of this shot spectrum $U(f)$ and our delay spectrum $R(f)$.

Our model reproduces some of the features within the data for blast C, but the correspondence is poor compared to blast B on August 7. Similar peaks occur at 8, 12, and 30

Hz in the model and spectrum for blast C; however, the spectral peak between 50 and 60 Hz within the model is absent in the data (the 60 Hz peak in the P_n spectrum is noise). The spectral peak near 20 Hz does not coincide with one in the model. At frequencies lower than 4 Hz the model is greater than the P_n spectrum. Some of these differences could originate from local site effects or in the spectrum $U(f)$ from a single shot. Likely random variations in the shooting delays would have only a minor effect on the fundamental 52 Hz spectral reinforcement (Winzer *et al*, 1979). Instead, the absence of the primary reinforcement between 50 and 60 Hz in P_n may be indicative of path attenuation. The next section reconciles the absence of a 52 Hz spectral reinforcement within the P_n phase using both intrinsic and scattering attenuation

Constraints on Propagation

The efficacy of high frequencies for detection and discrimination of chemical explosions, nuclear explosions, and earthquakes depends on their efficient propagation over regional distances, say 100 to 1500 km. Near source observations suggest efficient propagation of high frequencies over short distances within the continental shield. A local explosion conducted for road excavation near Balmertown at a distance of 20 km from our site shows numerous crustal phases and a high SNR. A presumed corner frequency occurs at 50 Hz, and high frequencies decay at $f^{-4.5}$ in displacement amplitude, although both could be artifacts of ripple-firing or path attenuation, the f_{max} problem (Hanks, 1982). The data does suggest efficient propagation to at least 70 Hz. This is not surprising; Frantti (1962) observed mining blasts to 50 Hz at distances greater than 100 km. Our critical parameter for detection, the signal-to-noise ratio (SNR), also peaks between 50 and 70 Hz. This is a simple consequence of the apparent corner frequency and the consistent f^{-2} decrease in seismic noise.

Observations of strong spectral reinforcements near 20 and 28 Hz indicate propagation to at least 400 km for these frequencies. No spectral peak is evident for blast C where the reinforcement should occur near 52 Hz, according to our model in Figure 7b; either the signal is strongly attenuated or unpredicted irregularities in the delays between rows suppress the expected reinforcement. However, random variations applied to delay times within the blast pattern still produce a strong 52 Hz spectral reinforcement, which bars the latter mechanism.

If path attenuation removes the spectral reinforcement at 52 Hz for blast C, a comparison of the model to the observed spectrum suggests attenuation by a factor of 30 over the propagation path. But the difference at 30 Hz is only a factor of 3. Assuming Q is

constant with frequency, the amplitude is proportional to

$$A(f,x) = S(f)A_0(x)\exp(-\frac{\pi f x}{Qv})$$

where f is the frequency, x is the distance between the station and source, v is the velocity of the medium, $A_0(x)$ incorporates geometrical spreading, and $S(f)$ represents the source spectrum. The attenuation could represent a combination of scattering attenuation, Q_S, and intrinsic attenuation, Q_I, such that

$$\frac{1}{Q} = \frac{1}{Q_I} + \frac{1}{Q_S}$$

(Dainty, 1981; Wu, 1982; Richards and Menke, 1983). Using this relationship and comparing the observed spectrum for blast C to its model at 52, 30, 12, and 8 Hz in Figure 7b suggest values for Q between 1500 and 5000. These values are strongly dependent on the high frequency behavior of a single shot (*e.g.*, f^{-2} or f^{-3}) and how Q influences spectral peaks at 8 Hz and 12 Hz. Modulations introduced by ripple-firing are superimposed upon the high frequency behavior of a single shot; if we were to ignore these modulations, fitting the observed data to a f^{-2} model between 10 and 40 Hz would give an erroneous estimate of the total path Q. This effect is a clear danger for attenuation estimates when using unknown chemical explosions as sources for propagation studies.

If the attenuation originates from scattering, a comparison of spectra from the direct P_n arrival and its coda should indicate increasing energy in the coda as frequency increases (Richards and Menke, 1983). Figure 8a shows P_n for blast C on August 6 and the later P_g arrival. Between the two arrivals lies the coda for P_n, and it shows much higher frequencies than the direct P_n phase. The spectra in Figure 8b emphasize the difference between the direct arrival P_n and its coda prior to P_g. Frequencies between 20 and 70 Hz show a 10 db increase in the coda relative to the direct arrival. Moreover, the coda spectrum now suggests the presence of a 52 Hz reinforcement which is predicted by our model. Frequencies less than 20 Hz show lower amplitudes in the coda. This spectral behavior agrees with scattering as the attenuation mechanism.

Frankel and Wennerberg (1987) proposed an *energy-flux model* for the separation of scattering and intrinsic attenuation in the seismic coda. They applied the model to the duration of the S-wave coda following a local earthquake. Using their formulation linking the coda amplitude to the energy in the direct wave for a 3-D medium, we obtain the frequency-dependent partitioning of energy between the coda and the direct arrival. The ratio R_{CD} represents the spectral amplitude density of the coda to the square root of the *total energy* in the direct arrival:

$$R_{CD} = \sqrt{3}t_d t^{-3/2} e^{-\frac{\pi f(t-t_d)}{Q_I}} e^{\frac{\pi f t_d}{Q_S}} \sqrt{1 - e^{-\frac{2\pi f t}{Q_S}}}$$

where t_d is the travel time for the direct arrival, t represents the travel time for the coda, Q_I denotes the intrinsic attenuation, and Q_S is the scattering attenuation. The spectral amplitude density in the coda is computed within a window which excludes contaminating phases; the total energy within the direct arrival is the product of the energy density within a window limited to the direct arrival and the window length.

We can reformulate these results and simplify them to explain the frequency content of the P_n coda at regional distances. The short duration (*200 ms*) of blast C on August 6 allows the separation of the direct arrival from the coda; we observe a sharp transition from the P_n phase to its coda in Figure 8a. Any Q determined would still be a combination of scattering near the surface and along the deeper path. Using the P_n coda prior to P_g for regional events minimizes contamination of the coda by other seismic phases and implies that travel times for the coda and signal are almost equal. The previous relation for R_{CD} is then greatly simplified if $t - t_d \ll t_d$. This condition is met for our previous explosion C: the travel time is approximately 60 seconds for P_n, and the difference is 4 seconds. The first exponential term uses the travel time difference and has little impact on our frequency band for Q_I greater than about 3000; we therefore ignore it. The last two exponential terms only depend upon Q_S. We can then simplify our relationship for R_{CD} to

$$R_{CD} = \sqrt{\frac{3}{t}(e^{\frac{2\pi t f}{Q_S}} - 1)}$$

Thus, the ratio of the coda to the direct arrival should have a simple dependence on frequency: as the frequency increases, a larger proportion of the energy arrives as scattered energy. At high frequencies, this proportion can exceed the energy within the direct arrival itself. This is what we observe for frequencies greater than 20 Hz. Notice that this simplified model totally eliminates the effect of intrinsic attenuation Q_I, and, using the ratio of the coda and signal spectra for a regional event, isolates the scattering component of attenuation. This differs from the results of Frankel and Wennerberg (1987) for the duration of the coda.

Our simplified scattering model predicts the frequency content of the coda for spectra in Figure 8b. Using the amplitude ratio of the P_n direct arrival to its coda, we obtain a frequency dependence for the spectral ratios which is equivalent to R_{CD}. As in our theoretical model, this ratio should only include the influence of scattering, and it removes intrinsic path attenuation common to both the direct wave and coda. Figure 8c plots the observed spectral ratio and compares it to the predicted values using a scattering Q_S of *5000* and *2500*. As the frequency increases, the amount of energy scattered out of the direct wave and into the coda increases, and thus our ratio increases with frequency. This is predicted by the model and observed in the data. At frequencies higher than 65 Hz the P_n signal is lost in the noise; this is consistent with the observed ratio and invalidates

any further comparisons to the model at higher frequencies. For frequencies lower than 5 Hz the coda is lost in the expected background noise, while below 3 Hz the signal also approaches the pre-event background noise. Thus, useful comparisons are possible between 5 Hz and 60 or 70 Hz. The figure indicates that scattering Q_S of 2500 and 5000 bracket our observed ratio within this bandpass. The model also gives the best fit to the shape of the curve within this range of Q_S; therefore, ignoring our scaling factor, $\sqrt{3/t}$, would still yield similar values.

Numerous assumptions are inherent in this comparison. The theoretical development advanced by Frankel and Wennerberg (1987) assumes forward scattering within a 3-D volume, but P_n represents a guided wave. Fortunately, the differences between their 3-D and 2-D derivations are insignificant when using the spectral ratios of the coda to the direct phase for regional events. We might expect a large proportion of the scattering to occur during its transit through the crust, both near the source and near the receiver. Conversions from P to S near the source are unimportant since the converted phases would arrive much later, but conversions near the receiver would contaminate the coda with converted phases. The theoretical development, however, does not include the effect of any converted phases. The inclusion of converted phases would effectively lower Q_S or increase the scattering attenuation; energy is being scattered which we are not observing on the vertical seismometer. Our values of Q_S, 2500 to 5000, must then be considered an upper bound for the actual value.

If Q_S is near 2500, scattering attenuation may be responsible for the majority of the observed path attenuation derived from our previous comparison of the P_n spectrum to its model for blast C in Figure 7b; that estimate gave a total path Q between 1500 and 5000. If Q_S dominates the attenuation, converted phases may be significant and effect the coda as seen at NORESS (Dave Harris, personal communication); significant P to S conversions imply a much smaller Q_S, which contradicts our estimate for the total path Q. Finally, if scattering is the predominant mode of attenuation, intrinsic attenuation may be much smaller than scattering attenuation. This suggests a *minimum* value of 2500 for Q_I, the intrinsic attenuation.

If scattering dominates path attenuation, then a longer window to include both the direct P_n arrival and its coda will give a better estimate of the intrinsic attenuation, Q_I. Scattered energy from P_n would then be included in the final spectrum, thereby increasing the energy density at high frequencies and minimizing the impact of Q_S. To avoid contamination from other phases, our window can only extend to the P_g phase; we still lose scattered energy arriving at later times. Figure 8d compares the resulting spectra, which includes both P_n and its coda (until the P_g phase), to our model of ripple-firing after a Q correction. We now observe a much better correspondence than found in Figure 7b, and the minimum intrinsic attenuation represented by Q_I increases to approximately 6000.

This must be considered a *minimum* Q_I since we only include the first 5 seconds of the P_n coda. Our greatest deviation still occurs at 52 Hz, but now the difference is only a factor of 3 in amplitude at the expected spectral reinforcement. The best fitting model is only possible using a high frequency asymptote of f^{-2} for a single shot. This analysis suggests a marked decrease in our estimates of intrinsic attenuation after the inclusion of the scattered energy within the coda. Using the full coda would probably show a further increase in Q_I, that is, a further decrease in the observed intrinsic attenuation.

These results suggest that attenuation due to scattering dominates for regional events within a shield environment. Longer windows for spectral analysis of the direct arrival include scattered energy in the coda, minimize the effect of scattering, and thereby give a better estimate of the source properties; however, if these windows overlap other seismic phases, the results are suspect. Testing these hypotheses and verifying our estimates of Q_S and Q_I will require multiple measurements of P_n at increasing distances from the blasts (*e.g.* Smith, 1988).

The application of seismic high frequencies for detection still relies on the total path attenuation Q. Evernden *et al* (1986) assume a value of Q much higher than 5000 for their detection estimates of small explosions. This was not observed at RSON. The scattering Q_S of 2500 to 5000 appears to be the greatest problem; the energy is dispersed into the coda of the direct arrival and no longer contributes to a distinct onset of the phase. The result is the same as an equivalent intrinsic attenuation; the amplitude of the direct arrival at high frequencies is decreased, which lowers our signal-to-noise ratio for detection.

CONCLUSIONS

These studies suggest the existence of a distinctive signature for large chemical explosions: strong, high-frequency spectral peaks in the P spectra introduced by delay shooting or ripple-firing. This signature might be useful for the identification of chemical explosions, but its application to seismic verification has a number of caveats:

1. Large chemical explosions must be ripple-fired for the existence of this spectral signature. Ripple-firing (or delay-shooting) is the international norm for efficient fragmention of rock.
2. The shooting pattern and delay parameters must be conducive to large spectral reinforcements in the seismic bandwidth; for useful discrimination of chemical explosions this bandwidth must extend to at least 35 or 40 Hz at regional distances. Short delay times, say 17 ms (*or 59 Hz*), give spectral reinforcements which may be strongly attenuated during propagation and thus unobservable at regional distances within the direct P_n arrival. Stations placed within a few hundred kilometers of a mining region would benefit from even a greater seismic bandwidth.
3. Seismic noise within this bandwidth must be predictable, low, and free from large spectral lines which characterize mechanical sources.
4. For P propagating to 20 km distance in a continental shield, negligible attenuation occurs to at least 70 Hz. At 400 km, we observe negligible attenuation to at least 20 Hz. Spectral reinforcements from ripple-firing are still clearly observed to 30 Hz, but at 50 Hz the evidence suggests severe scattering.
5. For frequencies lower than 30 Hz, the comparison of spectral models for delay shooting and observed P_n spectra suggest a total $Q \approx 2500$ using a high frequency asymptote of f^{-2} for a single shot within the blast pattern, but Q could be as low as 1500 assuming frequency independence. These attenuations will limit the value of high frequencies for the detection of small decoupled explosions at large regional distances.
6. Estimates of path attenuation using a simple source model (*e.g.* f^{-2} or f^{-3}) for mine blasts will give erroneous values of Q; it would ignore modulations in the source spectra introduced by the blast pattern and delay times.

Our discussion suggests possible directions for future research. Resolving the attenuation characteristics at high frequencies requires observations of known, high frequency sources along a profile (Smith, 1988). If a 50 to 60 Hz reinforcement originates at the source, spectral ratios using sites along the profile would confirm the mechanism for attenuation, scattering or intrinsic.

ACKNOWLEDGMENTS

Numerous individuals contributed to the deployment of instruments near Red Lake, Ontario; they included Don Rock, Larry Wethern, Don Watwood, and Fred Followill. Special thanks go to Dave Harris for his data from the regional array, and to Randy Grose for programming and running the models on the mine blasts while supported by U.C. Berkeley under a joint Institute of Geophysics and Planetary Physics grant from LLNL. Norm Burkhard, Keith Nakanishi, Paul Kasameyer, Steve Taylor, and Dave Harris reviewed the manuscipt. Work performed under the auspices of the U.S. Department of Energy by Lawrence Livermore National Laboratory under Contract W-7405-Eng-48.

TABLE 1.

Mine Blasts

Mine Blast	Date	Location (Lat.) (Long.)	Total Explosive (kg)	Duration (ms)	Explosive (kg/ms)	Delays (ms) Major to Minor
A	July 31, 1985 1600 GMT	47.4N 93.1W	127,000	1260	100.	35, 25
B	Aug 7, 1985 1636 GMT	47.6N 92.6W	54,500	1250	43.5	50, 65, 35, 25
C	Aug 6, 1985 1638 GMT	47.7N 91.9W	132,500	207	640.	17, 9

Figure 1. Map view near Red Lake, Ontario, showing the locations of RSON, the temporary regional array (*crosses in inset*), and the site of the high-frequency field station (*HF and solid triangle*). Hardrock sites from the array are denoted by their station number. In addition, potential noise sources are also identified on the map: the data trailer for the array (*tr*), microwave tower (*tw*), dump site (*du*), and adjacent rock quarry (*qu*). Directions and distances to the Griffith Mine and the mines in Balmertown and Madsen are shown on the larger area map. The map also shows the principal lakes (*shaded areas*), powerlines (*dashed line*), and highways (*identified solid lines*).

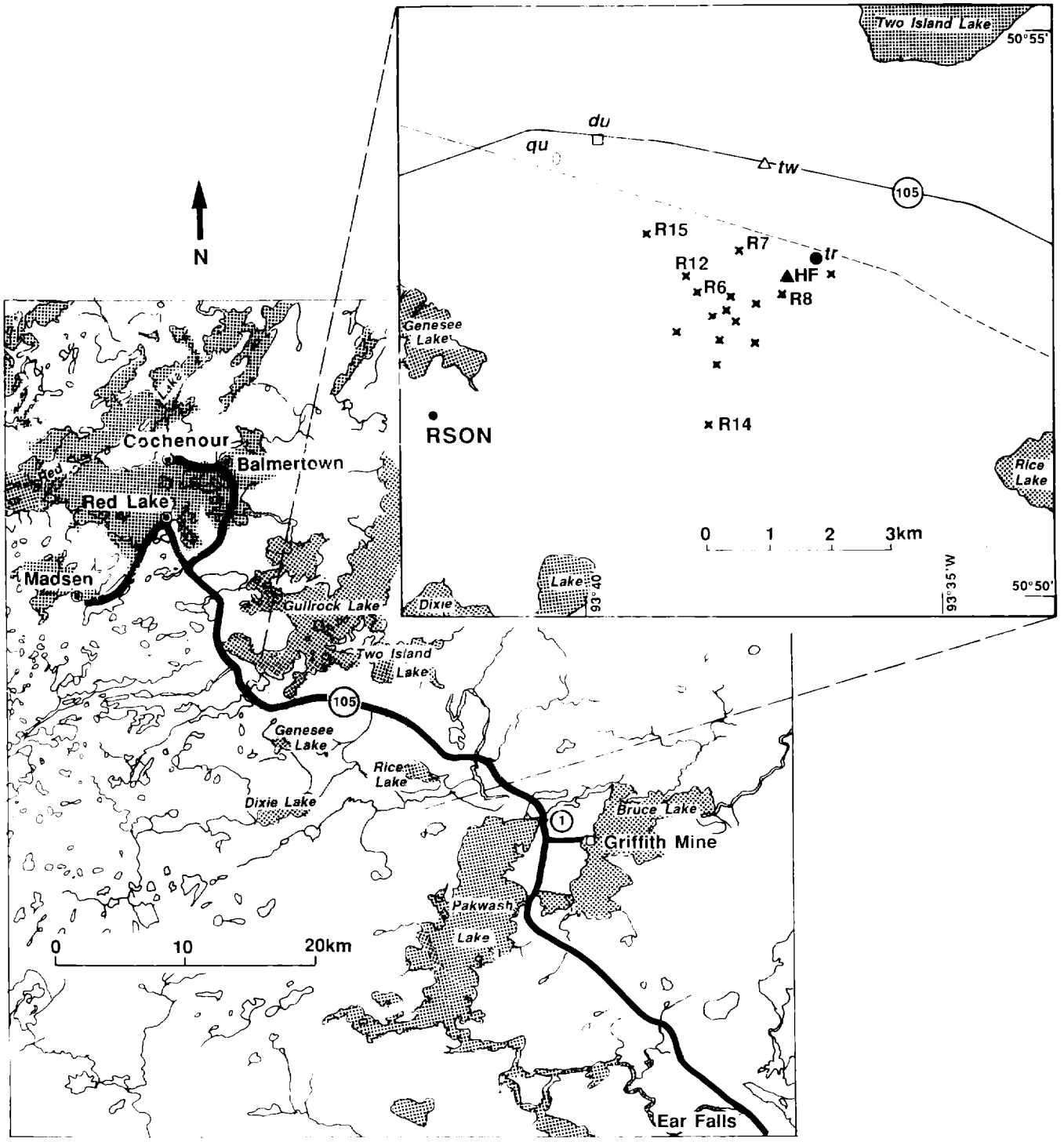
Two Island Lake
50°55'
du
qu
tw
105
R15
R7
tr
R12
HF
R6
R8
N
Genesee Lake
RSON
R14
Rice Lake
0 1 2 3km
93°40'
93°35'W
50°50'
Lake
Dixie
Cochenour
Balmertown
Red Lake
Madsen
Gullrock Lake
Two Island Lake
105
Genesee Lake
Rice Lake
Dixie Lake
Bruce Lake
1
Griffith Mine
Pakwash Lake
0 10 20km
Ear Falls

Figure 1.

Figure 2. A model illustrating ripple-firing (delay-shooting) of a mine blast. The top diagram plots the occurence of six separate explosions with time t. Each explosion is successively delayed by δ_t and the total duration of the blast is $t_N = 6 \cdot \delta_N$. This is equivalent to the application of a box-car of length t_N to a comb function with intervals of δ_t. Transforming to the frequency domain in the lower diagram gives periodic reinforcements at multiples of the comb frequency, $\frac{1}{\delta_t}$. The blast duration determines the width of the spectral peak, $\frac{2}{t_N}$, and the ripples between reinforcements.

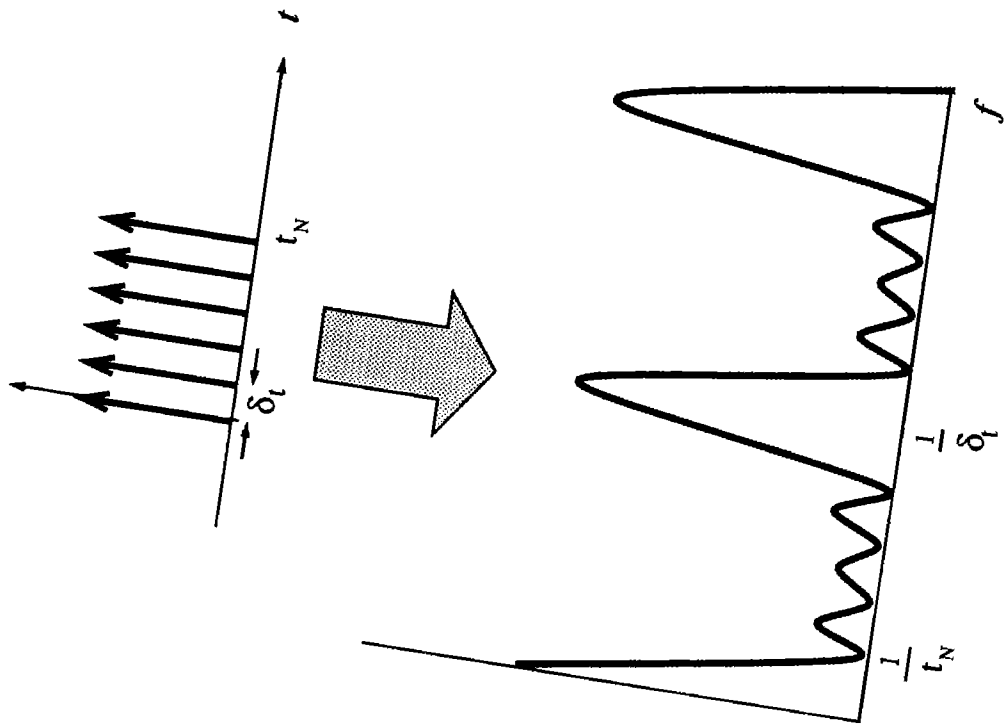

Figure 2.

Figure 3. Unfiltered and bandpassed seismograms for two ripple-fired explosions within the Mesabi Iron Range of northern Minnesota. The unfiltered response is flat from 1 to 125 Hz in velocity. To the left of each trace is the bandpass of the two pole filter.

a. Seismograms for ripple-fired explosion **A** on July 31, 1985. The explosion was at a distance of 390 km, and had predominant delays of 35 ms, a total explosive charge of *127,000* kg., and a duration of 1.26 seconds. The best SNR for P_n occurs between 16 and 32 Hz.

b. Seismograms for ripple-fired explosion C on August 6, 1985. The explosion occurred at a distance of 380 km. The event was recorded as two separate triggers: the first on the P_n phase and the second on the L_g phase. The predominant delay used for ripple-firing was 17 ms; the total duration was 207 ms; and the total explosive was *132,500* kg. The velocity seismograms show a strong P_n and P_g phase, and following a break, L_g (*at 55 seconds*) and R_g (*at 70 seconds*). For P_n the best SNR occurs between 4 and 8 Hz; for L_g the best SNR lies between 1 and 2 Hz; and the best SNR for R_g occurs between .25 and 1 Hz. The P_n coda within the 32 to 50 Hz bandpass resembles a lunar seismogram and suggests strong scattering.

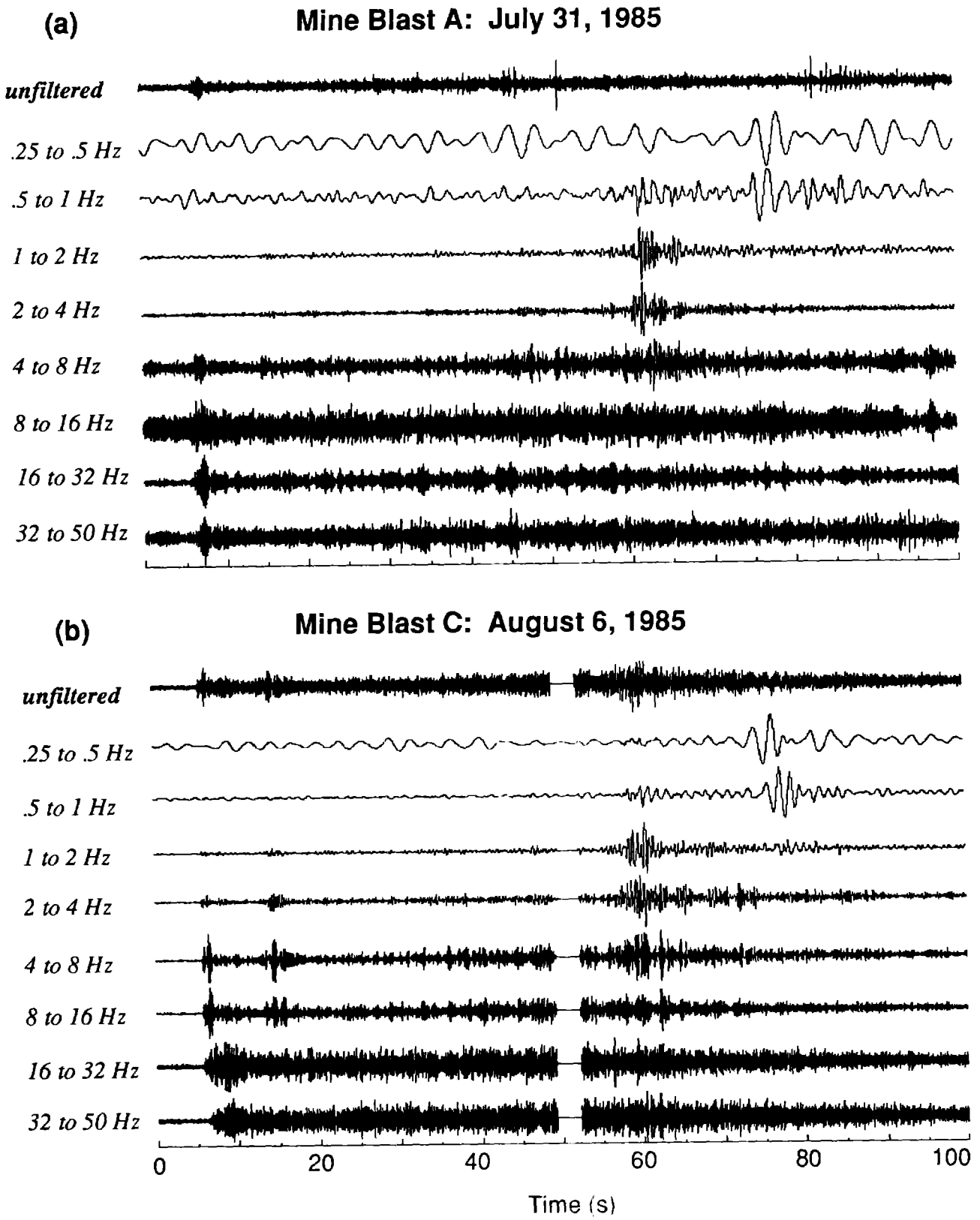
(a)
Mine Blast A: July 31, 1985
unfiltered
.25 to .5 Hz
.5 to 1 Hz
1 to 2 Hz
2 to 4 Hz
4 to 8 Hz
8 to 16 Hz
16 to 32 Hz
32 to 50 Hz
(b)
Mine Blast C: August 6, 1985
unfiltered
.25 to .5 Hz
.5 to 1 Hz
1 to 2 Hz
2 to 4 Hz
4 to 8 Hz
8 to 16 Hz
16 to 32 Hz
32 to 50 Hz
0
20
40
60
80
100
Time (s)

Figure 3.

Figure 4. Displacement power density spectra for P_n and pre-event noise for three mining blasts in Table 1. All occur in the Mesabi Iron Range at a distance of 380 to 390 km. Each spectrum uses a single 2 second window with pre-whitening for the correlation function and a 0.5 second window for the smoothed power density estimate. Shown above each spectrum is the power signal-to-noise ratio.

a. Spectra for mine blast **A**: The best SNR (*power*) corresponds to a strong spectral reinforcement in P_n near 26 Hz. This spectral reinforcement agrees with the 35 ms delay between the rows within the blast pattern.

b. Spectra for mine blast **B**: The P_n spectra shows a strong 20 Hz spectral reinforcement which coincides with the maximum SNR. The predominant delay between rows in the blast was 50 ms, the total duration was 1.25 seconds, and the total explosive charge was *54,500* lb. Unlike the previous record, this data is from site R08 of the array, the same granitic outcrop as the high frequency site. Frequencies above 35 Hz are strongly biased by the anti-aliasing filter and are not reliable. As before, the data was recorded as acceleration.

c. Spectra for mine blast **C**: The maximum (*power*) SNR corresponds to the apparent corner frequency of the P_n phase. At high frequencies, the P_n signal decreases as f^{-4} in displacement amplitude. Powerline interference at 60 Hz is apparent in both noise and signal spectra. Delays between rows are now shorter, 9 and 17 ms.

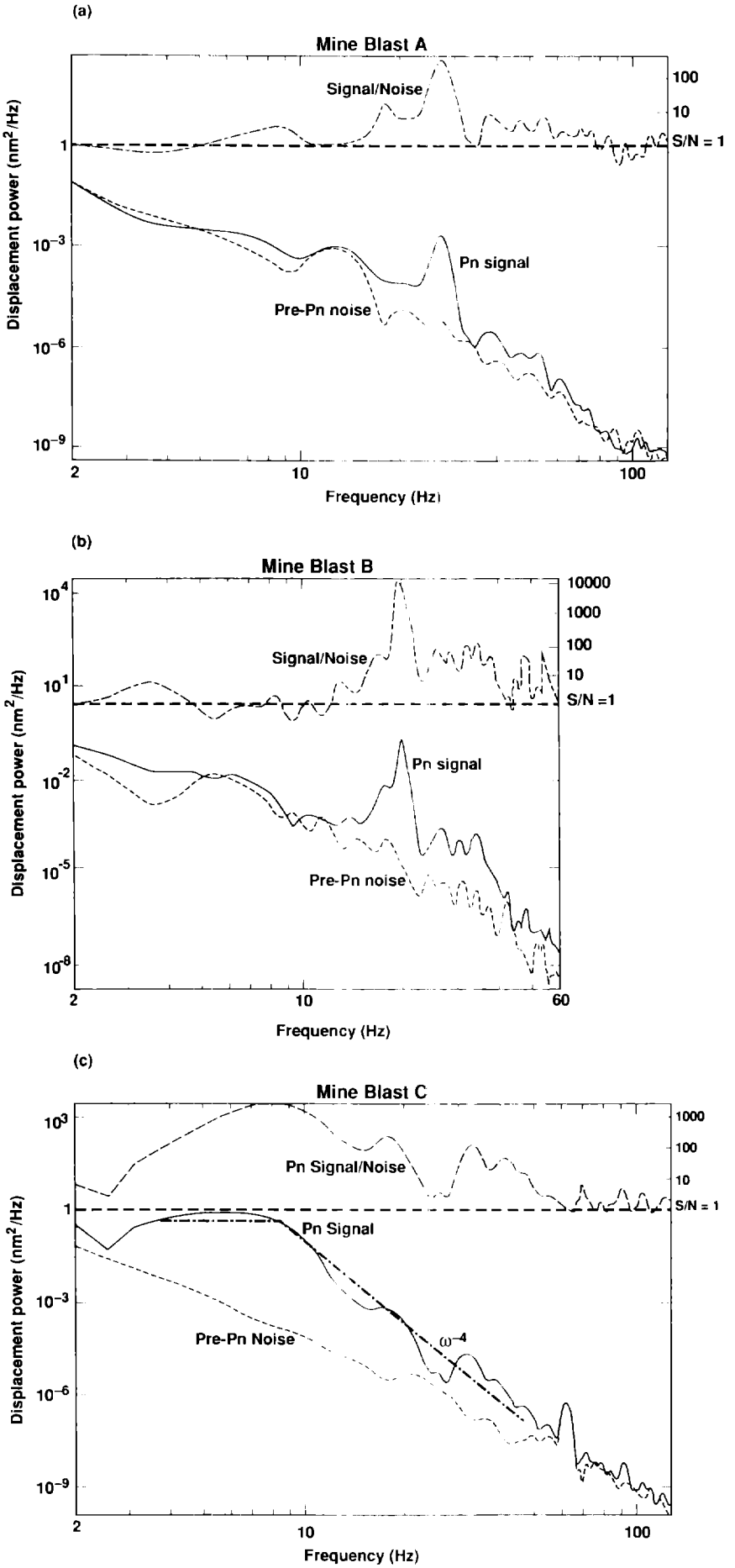
(a)
Mine Blast A
Signal/Noise
100
10
S/N = 1
1
10^{-3}
10^{-6}
10^{-9}
Pn signal
Pre-Pn noise
Displacement power (nm^2/Hz)
2
10
100
Frequency (Hz)
(b)
Mine Blast B
10^4
10^1
10^{-2}
10^{-5}
10^{-8}
10000
1000
100
10
S/N =1
Signal/Noise
Pn signal
Pre-Pn noise
Displacement power (nm^2/Hz)
2
10
60
Frequency (Hz)
(c)
Mine Blast C
10^3
1
10^{-3}
10^{-6}
10^{-9}
1000
100
10
S/N = 1
Pn Signal/Noise
Pn Signal
Pre-Pn Noise
ω^{-4}
Displacement power (nm^2/Hz)
2
10
100
Frequency (Hz)

Figure 4.

Figure 5. Comparison of P_n spectra for the previous ripple-fired mining explosion C (*solid line*) on August 6, 1985; refraction shot (*dotted line*) on September 25, 1984, at 0400 GMT; and M_L 4.4 earthquake (*dashed line*) on March 4, 1983, at 0632. The distance of the mining explosion was 380 km; the refraction shot was 290 km from RSNY, the site of the recording; and the earthquake was recorded at RSON, a distance of 900 km. The two-ton refraction shot was part of the USGS Maine experiment and was conducted in the bottom of a water filled quarry. Thus, the shot may have generated a strong bubble pulse or similar resonance within the water or quarry. If the corner frequency of the earthquake is taken as 4.5 Hz, the high-frequency asymptote is near f^{-2} in displacement amplitude. The refraction shot is closer to f^{-3}, and the mine (*quarry*) blast appears closer to f^{-4}.

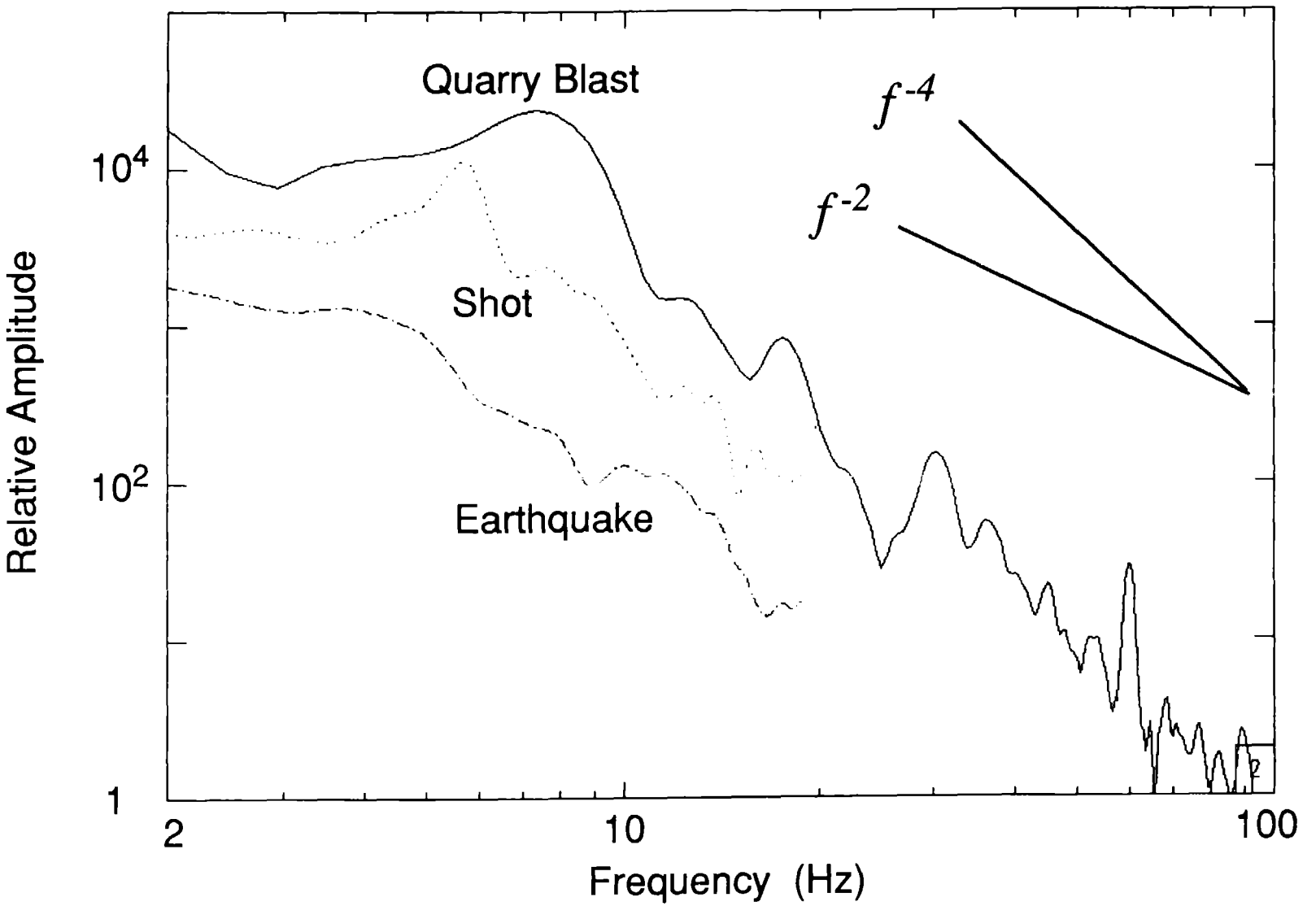
Quarry Blast
f^{-4}
f^{-2}
Shot
Earthquake
10^4
10^2
1
Relative Amplitude
2
10
100
Frequency (Hz)

Figure 5.

Figure 6.

a. Map view of shooting pattern for mine blast **B** on August 7, 1985. The coordinates are in kilometers with north at the top of the diagram. Each shot hole is denoted by an asterisk, and shot holes detonated simultaneously as a row are connected by a solid line. Between rows is specified a delay time: near the initiation point the delays are short, 25 ms and 35 ms; the major portion of the pattern uses 50 ms delays between rows; but in the last seven rows the delay increases to 65 ms. Each shot hole is 10 m deep and holds an average charge of 400 kg. of explosive.

b. Ripple-fired delay function $r(t)$ for an azimuth of 341°, which corresponds to RSON. Cummulative charge in kilograms per millisecond is plotted against the shot delay time. For a vertical propagating wavefront, all shots within a row would accummulate at the same millisecond; the finite spatial pattern and the non-vertical take-off angle for a ray smears the accumulation of a row over about 20 ms. The spatial pattern has little effect on low frequencies (*e.g.* 50 ms separation between rows), but reduces high frequency harmonics. A gradual decrease in charge size per hole is evident toward the end of the blast pattern.

c. Spectrum of ripple-fired delay function $r(t)$ for two azimuths, 251° for RSSD and 341° for RSON. The plot represents power density per Hz of the previous cummulative charge. There is little difference between the two azimuths. Strong spectral reinforcements occur at 20 Hz and at higher harmonics of 40, 60, and 80 Hz in this plot. The finite spatial pattern tends to suppress the higher frequencies.

d. Comparison of acceleration power density spectra for P_n and model of ripple-fired mining explosion **B**. The P_n spectra is derived from Figure 4b, and the model from Figure 6c. Both use the same spectral estimation. The ordinate of the model is scaled by 10^4 so as to overlay the P_n spectra. In addition, the model assumes a high-frequency asymptote of f^{-2} in displacement amplitude (*flat to acceleration*) for a single shot within the blast.

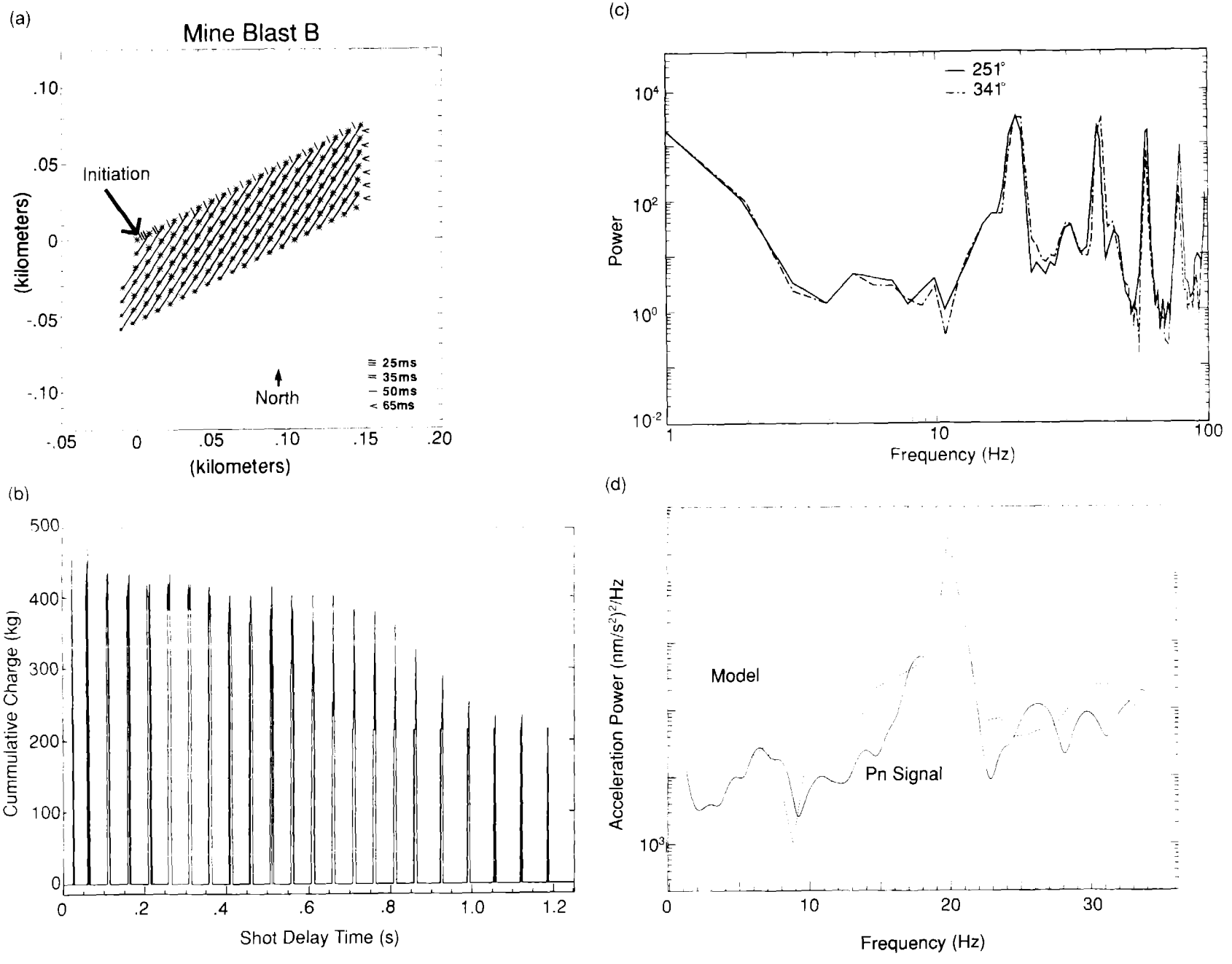
(a)
Mine Blast B
.10
.05
0
-.05
-.10
(kilometers)
Initiation
North
≡ 25ms
= 35ms
– 50ms
< 65ms
-.05
0
.05
.10
.15
.20
(kilometers)
(b)
500
400
300
200
100
0
Cummulative Charge (kg)
0
.2
.4
.6
.8
1.0
1.2
Shot Delay Time (s)
(c)
— 251°
--- 341°
10^4
10^2
10^0
10^{-2}
Power
1
10
100
Frequency (Hz)
(d)
Model
Pn Signal
10^3
Acceleration Power (nm/s^2)^2/Hz
0
10
20
30
Frequency (Hz)

Figure 6.

Figure 7.

a. Map view of shooting pattern for mining blast C on August 6, 1985. The configuration is much more complex: the blast propagates outward in a chevron pattern from the initiation point. Again, individual shot holes are denoted by asterisks, and are grouped into rows by a solid line. The shots in each row fire essentially simultaneously. The first four delays from the initiation point are 9 ms, and this short delay continues for the rest of the northern portion of the pattern. The southern portion of the chevron continues with 17 ms delays. As a result, the total duration of the blast is very short for an explosion of this size, only 200 ms. The hole depths range from 8.5 to 18 meters, and the corresponding charges for each hole vary from 600 to 1900 kg. (a shallower hole has a smaller charge). The total explosive is 132,500 kg.

b. Comparison of the P_n spectrum (*solid line*) for blast C to the theoretical spectrum $G(f)$ for the blast (*dotted line*). Both are in acceleration power density. The P_n spectra uses a two second window and only includes the direct arrival. The model assumes the spectra $U(f)$ for a single shot has a corner frequency of 6 Hz and a high frequency asymptote which is flat to acceleration (f^{-2} in displacement amplitude). The delay spectra $R(f)$ is again scaled by 10^4. There is little evidence for the 52 Hz spectral reinforcement in the P_n spectra, but spectral peaks coincide at 8, 12, and 30 Hz.

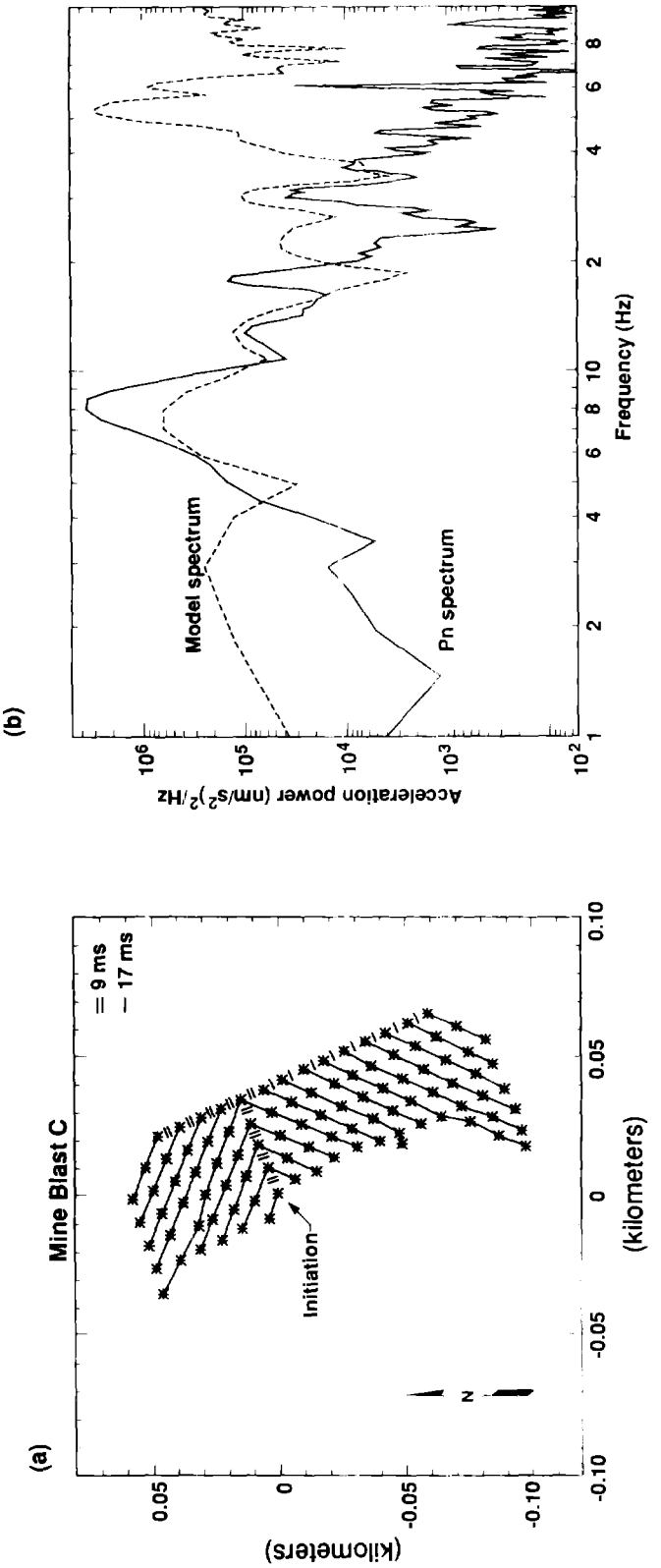
(a)
Mine Blast C
= 9 ms
– 17 ms
Initiation
N
(kilometers)
0.05
0
-0.05
-0.10
0.10
(b)
Acceleration power (nm/s²)²/Hz
Model spectrum
Pn spectrum
Frequency (Hz)
10⁶
10⁵
10⁴
10³
10²
1
2
4
6
8
10

Figure 7.

Figure 8.

a. Seismogram showing P_n, P_n coda, and P_g for the mining blast C on August 6, 1985 (*see Figure 3b*). To emphasize high frequencies, acceleration is plotted. The P_n arrival continues for approximately 1.5 seconds; seven seconds later begins the largest P_g phase. The P_n coda has a much higher frequency content than either P_n or P_g. The P_n coda extends from 2 to 7 seconds following the initiation of P_n.

b. Spectra for direct P_n arrival (*solid line*) and later P_n coda (*dotted line*) for the explosion C in Figure 7 on August 6, 1985. Both spectral estimates use 2 second windows for the correlation function. The P_n spectrum uses one window; the coda uses three windows and averages them. The results are smoothed using a 1 second window for the power density estimate. Other combinations have little effect on the spectra. The power within the coda exceeds the direct arrival for frequencies above 20 Hz, as expected for scattering. Frequencies below 5 Hz and above 65 Hz are in the background noise. The large spectral hole in P_n at 24 Hz might be a site phenomena. A 52 Hz peak appears in the coda spectra, and 60 Hz noise occurs in both.

c. Amplitude ratio (*solid line*) of P_n coda spectrum to P_n spectrum with comparisons to forward scattering models (*dotted lines*). The amplitude ratio is computed from the spectra in Figure 8b and is plotted as a *solid line*. Frequencies below 5 Hz and above 65 Hz are biased by the background seismic noise. The ratio is compared to two different scattering attenuations, Q_S of *2500* and *5000*. These scattering Q's bracket the spectral ratio.

d. Comparison of P_n plus coda spectra (*solid line*) to theoretical models with intrinsic path attenuation Q_I (*dotted lines*). The spectral estimation for the combined coda and direct P_n arrival uses a seven second window beginning at P_n. Intrinsic path attenuation is applied to the theoretical blast spectra in Figure 7b. Models assume a f^{-2} high-frequency asymptote for a single shot. The closest fit is now achieved with an intrinsic Q_I of 6000.

regional seismic test network from 0.1 to 20 hz, *Bull. Seis. Soc. Am.* **77**, 663-678.

Sharpe, J.A. (1942). The production of elastic waves by explosion pressures: I, Theory and empirical field observations, *Geophysics* **7**, 144.

Smith, A.T. (1986). Seismic propagation at high frequencies across stable continental shields and platforms, *Earthquake Notes* **57**, 9.

Smith, A.T. (1987). Seismic site selection at high-frequencies: a case study, *Lawrence Livermore National Lab.*, UCID-21047.

Smith, A.T. (1988). High-frequency P-wave attenuation near the East Kazakh Test Site using a new method with spectral ratios, *Earthquake Notes* **59**, 45.

Smith, A.T., and R.D. Grose (1987). High-frequency observations of signals and noise near RSON: implications for the discrimination of rippled-fired mining blasts, *Lawrence Livermore National Lab.*, UCID-20945.

Taylor, S.R. (1981). Properties of ambient seismic noise and summary of noise spectrum in the vicinity of RSTN sites, *Lawrence Livermore National Lab.*, UCID-18928.

von Seggern, D., and R. Blandford (1972). Source time functions and spectra for underground nuclear explosions, *Geophys. J. R. astr. Soc.* **31**, 83-97.

Willis, D.E. (1963). A note on the effect of ripple-firing on the spectra of quarry shots, *Bull. Seism. Soc. Am.* **53**, 79-85.

Winzer, S.R., V.I. Montenyohl, and A. Ritter (1979). The science of blasting, in *Proceedings of the Fifth Conference on Explosives and Blasting Technique*, Society of Explosive Engineers Annual Meeting, St. Louis, Missouri, 7-9 February 1979.

Wu, R. (1982). Attenuation of short period seismic waves due to scattering, *Geophys. Res. Letters* **9**, 9-12.

REFERENCES

Anderson, D.A., S.R. Winzer, and A.P. Ritter (1982). Blast design for optimizing fragmentation while controlling frequency of ground vibration, in *Proceedings of the Conference on Explosives and Blasting Techniques*, Society of Explosive Engineers Annual Meeting, New Orleans, LA, 31 January to 4 February 1982.

Bouchon, M. (1982). The complete synthesis of seismic crustal phases at regional distances, *J. Geophys. Res.* **87**, 1735-1741.

Brigham, E.O. (1974). The Fast Fourier Transform, Prentice-Hall, N.J.

Dainty, A.M. (1981). A scattering model to explain seismic Q observations in the lithosphere between 1 and 30 Hz, *Geophys. Res. Letters* **8**, 1126-1128.

Evernden, J.F., C.B. Archambeau, and E. Cranswick (1986). An evaluation of seismic decoupling and underground nuclear test monitoring using high-frequency seismic data, *Rev. of Geophys.* **24**, 143-215.

Frankel, A., and L. Wennerberg (1987). Energy-flux model of seismic coda: separation of scattering and intrinsic attenuation, *Bull. Seis. Soc. Am.* **77**, 1223-1251.

Frantti, G.E. (1962). Short-period seismic noise, in *Problems in Seismic Background Noise*, Univ. of Michigan, VESIAC Advisory Report 4410-32-X.

Frantti, G.E. (1963). Spectral energy density for quarry explosions, *Bull. Seis. Soc. Am.* **53**, 989-996.

Greenhalgh, S.A. (1980). Effects of delay shooting on the nature of P-wave seismograms, *Bull. Seism. Soc. Am.* **70**, 2037-2050.

Hanks, T.C. (1982). f_{max}, *Bull. Seism. Soc. Am.* **72**, 1867-1879.

Langefors, U., and B. Kihlstrom (1963). The Modern Technique of Rock Blasting, John Wiley and Sons, N.Y.

Pollack, H.N. (1963). Effect of Delay Time and Number of Delays on the Spectra of Ripple-Fired Shots, *Earthquake Notes* **34**, 1-12.

Richards, R.G., and W. Menke (1983). The apparent attenuation of a scattering medium, *Bull. Seis. Soc. Am.* **73**, 1005-1021.

Rodgers, P.W., S.R. Taylor, and K.K. Nakanishi (1987). System and site noise in the

regional seismic test network from 0.1 to 20 hz, *Bull. Seis. Soc. Am.* **77**, 663-678.

Sharpe, J.A. (1942). The production of elastic waves by explosion pressures: I, Theory and empirical field observations, *Geophysics* **7**, 144.

Smith, A.T. (1986). Seismic propagation at high frequencies across stable continental shields and platforms, *Earthquake Notes* **57**, 9.

Smith, A.T. (1987). Seismic site selection at high-frequencies: a case study, *Lawrence Livermore National Lab.*, UCID-21047.

Smith, A.T. (1988). High-frequency P-wave attenuation near the East Kazakh Test Site using a new method with spectral ratios, *Earthquake Notes* **59**, 45.

Smith, A.T., and R.D. Grose (1987). High-frequency observations of signals and noise near RSON: implications for the discrimination of rippled-fired mining blasts, *Lawrence Livermore National Lab.*, UCID-20945

Taylor, S.R. (1981). Properties of ambient seismic noise and summary of noise spectrum in the vicinity of RSTN sites, *Lawrence Livermore National Lab.*, UCID-18928.

von Seggern, D., and R. Blandford (1972). Source time functions and spectra for underground nuclear explosions, *Geophys. J. R. astr. Soc.* **31**, 83-97.

Willis, D.E. (1963). A note on the effect of ripple-firing on the spectra of quarry shots, *Bull. Seism. Soc. Am.* **53**, 79-85.

Winzer, S.R., V.I. Montenyohl, and A. Ritter (1979). The science of blasting, in *Proceedings of the Fifth Conference on Explosives and Blasting Technique*, Society of Explosive Engineers Annual Meeting, St. Louis, Missouri, 7-9 February 1979.

Wu, R. (1982). Attenuation of short period seismic waves due to scattering, *Geophys. Res. Letters* **9**, 9-12.